

Liquid-in-gas droplet microfluidics; experimental characterization of droplet morphology, generation frequency, and monodispersity in a flow-focusing microfluidic device

This content has been downloaded from IOPscience. Please scroll down to see the full text.

2017 J. Micromech. Microeng. 27 075020

(<http://iopscience.iop.org/0960-1317/27/7/075020>)

View [the table of contents for this issue](#), or go to the [journal homepage](#) for more

Download details:

IP Address: 129.10.131.109

This content was downloaded on 14/06/2017 at 17:27

Please note that [terms and conditions apply](#).

You may also be interested in:

[Droplet based microfluidics](#)

Ralf Seemann, Martin Brinkmann, Thomas Pfohl et al.

[Dripping and jetting in microfluidic multiphase flows applied to particle and fibre synthesis](#)

J K Nunes, S S H Tsai, J Wan et al.

[A review of the theory, methods and recent applications of high-throughput single-cell droplet microfluidics](#)

Todd P Lagus and Jon F Edd

[PDMS droplet formation and characterization by hydrodynamic flow focusing technique in a PDMS square microchannel](#)

J Carneiro, E Doutel, J B L M Campos et al.

[The shape of a step structure as a design aspect to control droplet generation in microfluidics](#)

S P C Sim, T G Kang, L Yobas et al.

[Control of Droplet Generation in Flow-Focusing Microfluidic Device with a Converging-Diverging Nozzle-Shaped Section](#)

Jerry M. Chen, Ming-Che Kuo and Chien-Po Liu

[A monolithically three-dimensional flow-focusing device for formation of single/double emulsions](#)

Shih-Hao Huang, Wei-Heong Tan, Fan-Gang Tseng et al.

[From tubes to drops: droplet-based microfluidics for ultrahigh-throughput biology](#)

T M Tran, F Lan, C S Thompson et al.

# Liquid-in-gas droplet microfluidics; experimental characterization of droplet morphology, generation frequency, and monodispersity in a flow-focusing microfluidic device

Pooyan Tirandazi and Carlos H Hidrovo

Mechanical and Industrial Engineering Department, Northeastern University, 334 Snell Engineering Center, 360 Huntington Ave, Boston, MA 02115, United States of America

E-mail: [hidrovo@neu.edu](mailto:hidrovo@neu.edu)

Received 31 January 2017, revised 15 May 2017

Accepted for publication 30 May 2017


Published 13 June 2017



## Abstract

Microfluidic techniques for production of uniform droplets usually rely on the use of two immiscible liquids (e.g. water-in-oil emulsions). It has been shown recently that a continuous gas flow instead of a second liquid carrier can be used as an alternative approach in droplet microfluidics. In this work we experimentally investigate the generation of liquid water droplets within air in flow-focusing configurations. Over a wide range of flow conditions we identify six distinct flow regimes inside the microchannel: Co-flowing, Threading, Plugging, Dripping, Multi-Satellite Formation, and Jetting. Flow regimes and their transitions are plotted and characterized based on the Weber number ( $We$ ) of the system. We further investigate the impact of liquid microchannel size on the flow maps. Generation frequency, morphology, and monodispersity of the droplets are characterized in more detail in the Dripping regime. Generation frequency can be related to the product of the liquid and gas flow rates. However, droplet morphology (length and width) is more dependent on the gas flow rate. We demonstrate the production of monodisperse droplets ( $d < 100 \mu\text{m}$  and  $\sigma/d < 5\%$ ) up to kHz formation rates in liquid-gas microfluidic systems for the first time. The results of this work provide practical and useful guidelines for precise, oil-free delivery of ultra-small volumes of fluid which can be integrated in lab-on-a-chip systems for a variety of applications in biochemical research and material synthesis.

Keywords: microfluidics, droplets, flow focusing, flow regimes, liquid-gas microflow

 Supplementary material for this article is available [online](#)

(Some figures may appear in colour only in the online journal)

## Introduction

Continuous formation of highly-reproducible liquid droplets in microfluidic channels has been employed as a promising tool in a wide variety of areas ranging from lab-on-a-chip applications [1, 2] to material synthesis [3]. Microfluidic droplet generation systems fundamentally rely on creating dispersions of one fluid within a different fluid medium, most commonly forming aqueous liquid droplets in an immiscible liquid carrier oil [4–9]. Using a viscous liquid as the continuous phase in which droplets are generated and carried is the prevalent method of droplet generation in microfluidic systems. The relatively high viscosities ( $\sim 1\text{--}1000\text{ mPa}\cdot\text{s}$ ) of the liquids involved in the system, the small channel dimensions ( $\sim\mu\text{m}$ ), and the low flow rates ( $\sim\mu\text{l min}^{-1}$ ) result in Reynolds numbers ( $\text{Re} = \rho U D / \mu$ , where  $U$  is a characteristic velocity, and  $D$  represents a characteristic length scale) that are typically less than unity in these systems [10]. Similarly, the Weber number ( $\text{We} = \rho U^2 D / \sigma$ ), which compares inertia to surface tension, is also generally small. Consequently, in most of the conventional droplet-based microfluidic systems the effect of inertia forces are negligible in the drop formation [6, 11]. The Capillary number ( $\text{Ca} = \mu U / \sigma$ ), which compares interfacial tension and viscous forces, becomes the natural dimensionless parameter that characterizes the interaction between the two liquids in the breakup phenomena. In a broader perspective, for a range of  $\text{Ca}$  for each liquid, various flow breakup modes can be differentiated [12]. Characterizing and understanding these flow regimes plays an essential role towards tailoring droplet generation systems for creating monodisperse droplets, which is the ultimate goal of these microsystems.

Generation of liquid droplets within a gaseous flow in microfluidic networks is a newer approach to the conventional liquid-in-liquid systems. One of the main advantages of this approach for droplet formation is the possibility of creating uniform particles purely in air (monodisperse aerosols) and without the presence of a second liquid carrier. Therefore, the final product can be readily attained obviating extra washing steps to remove the carrier oil [13]. Moreover, generation of droplets in a liquid medium is usually facilitated by adding surfactants to the continuous liquid carrier. However, it is believed that using certain surfactants may impose usage limitations mainly due to cross-contamination of the droplet contents [14, 15]. Surfactants are clearly not required for droplet generation in a gaseous phase, ensuring preservation of the droplets' contents. Although some early works have investigated the breakup of a liquid jet into droplets using a focusing air in unconfined nozzle-like geometries [16–21], gaseous generation of monodisperse drops within a microfluidic system is an entirely different process due to confinement-induced effects [22]. Interaction of liquid and gas inside confined microchannel geometries has also been widely studied in the operation of proton exchange membrane fuel cells (PEMFC) [23–32]. However, droplet generation in gaseous microfluidic systems that employ similar architectures as those used in conventional oil-based systems has been the subject of a very few studies during recent years. The gas flow velocities required for droplet generation are at least an order-of-magnitude higher

than those employed when using a highly viscous oil phase. As such, inertial effects become more prominent and relevant in the fluid-fluid interactions of these systems. Droplet detachment has been numerically and experimentally investigated in a T-shaped junction under the introduction of a high-speed gaseous flow. It was demonstrated that the mechanism responsible for the breakup of the drops transitions from hydrodynamic pressure difference (arising from the microchannel confinement) at lower  $\text{Re}$  to inertial drag at higher  $\text{Re}$  as the gaseous flow increases [33, 34]. Confined generation of aqueous droplets has also been shown in a circular capillary co-flow system using gas as the continuous phase. Under relatively low liquid flow rates (less than  $1\ \mu\text{l min}^{-1}$ ) and gas velocities (below  $3\text{ m s}^{-1}$ ) uniform droplets between  $250\ \mu\text{m}$  and  $320\ \mu\text{m}$  were obtained within concentric hydrophobic glass capillaries [35]. More recently, confluence of liquid in a gaseous stream in various planar confined flow-focusing microgeometries was studied. It was shown that over a wide range of liquid and gas flow rates three main regions (i.e. Dripping, Jetting, and Stratified Flow) are observed within confined polydimethylsiloxane (PDMS) microchannels [36]. While this study provided useful insights regarding the dynamics of gas-liquid interactions in planar flow-focusing geometries, it did not address several key aspects of this system. For example, the monodispersity and characteristics of the droplets generated within the Dripping region was not presented. This is very relevant information towards the design of these systems since the Dripping regime is one of the two desirable modes of operation for droplet generation. Furthermore, neither study looked at the effect that flow conditions has on the droplet morphology or generation frequency in this flow regime.

In this study, we examine the aforementioned effects on droplet formation in a gas flow inside a microfluidic flow-focusing device with mixed hydrophobicity surface conditions. Unlike previous studies that used different surface chemical coatings to render the microchannel fully hydrophobic, we incorporated a mixed hydrophobic/hydrophilic PDMS-glass hybrid structure without chemical coatings. Six different flow regimes were distinguished and mapped in these mixed surface conditions structures: Co-flowing, Threading, Plugging, Dripping, Jetting, and Multi-Satellite Formation. The effect that microchannel size has on droplet formation is investigated towards the development of these richer flow maps. Particular attention is paid to the Dripping regime for the generation of uniform droplets. Droplet morphology, monodispersity, and generation frequency are characterized as functions of gas and liquid flow rates in this regime for the first time. Using this structure, we demonstrated uniform droplet generation over a wider range of flow conditions and smaller sizes (below  $100\ \mu\text{m}$ ) as compared to previous studies. The chip-based nature of this microfluidic module offers great opportunities for integration in more complex lab-on-a-chip systems for next generation of high-throughput airborne target screening and detection. Moreover, performing different chemical and biochemical microreactions within individual drops surrounded by air or other gases provide new opportunities in aerosol and aerobiology applications where interaction of gas and liquid phases is essential.

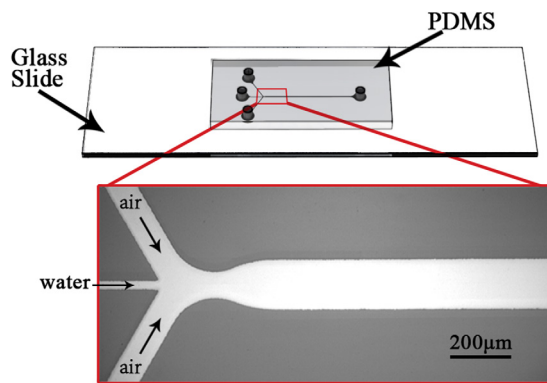


**Figure 1.** Schematic of the microfluidic device for water droplet formation in air. Liquid water is injected through the middle channel and meets the two side air streams at a flow-focusing junction. The final device is prepared by bonding PDMS chips to a glass slide. The microchannels' height is  $40\ \mu\text{m}$  for all the experiments.

## Experimental procedure

### Fabrication and preparation of microfluidic devices

We fabricated the microfluidic devices using standard photolithography process with SU-8 and soft lithography with PDMS [37]. Briefly, a silicon master mold containing channel features was fabricated using a negative photoresist (SU-8 2050 MicroChem Corp.) with  $40\ \mu\text{m}$  height. Once the silicon mold is fabricated, a PDMS solution is prepared from Sylgard 184 silicone elastomer kit (Dow Corning Corp.) with the ratio of 10:1. The mixture is poured onto the prepared silicon mold and is degassed in a vacuum chamber. The assembly is then baked at  $80\ ^\circ\text{C}$  for 2 h and once cured, the PDMS layer is peeled off the mold and each chip is cut out of the PDMS layer. Each device is then cleaned with DI water and is bonded to a pre-cleaned glass slide (Thermo Fisher Scientific Inc.) after being exposed to an oxygen plasma (Harrick Plasma Inc.). Finally, the chips are post-baked for 4 h at  $200\ ^\circ\text{C}$  and can be used for experiments after being cooled down to room temperature. The final device and the microchannel configuration is depicted in figure 1.

Wetting behavior of the microchannel walls plays a critical role in the performance of droplet-based microfluidic systems that use a planar architecture [38]. In conventional liquid-in-liquid systems the surface of the microchannels is modified to reduce droplet interactions with the walls. In other words, stable water-in-oil emulsions can be formed in hydrophobic microchannels and on reverse emulsions (oil-in-water) the microchannels should be hydrophilic (oleophobic). Although PDMS is intrinsically hydrophobic, the use of oxygen plasma for bonding renders them hydrophilic which makes liquid handling difficult within microchannels. Moreover, compatibility issues of PDMS surfaces with organic solvents [39], including a variety of the oils used in droplet-based systems, pose additional challenges for droplet generation in liquid-liquid systems. Obtaining the conditions that suit the generation process is usually achieved by manipulating the microchannel surfaces through chemical coatings. A variety of techniques and chemicals are employed to achieve the

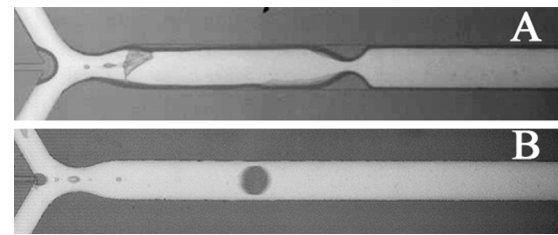


**Figure 2.** Interaction of liquid and gas in different channel conditions. (A) After plasma treatment; in this situation channels are hydrophilic and as a result the liquid water tends to adhere to the side walls of the microchannel once it enters the junction. (B) After post-baking step; here the PDMS has regained its hydrophobic nature and droplets maintain their morphology after generation.

**Table 1.** Measured contact angles for ten samples of PDMS and glass substrates with the same preparation conditions of plasma treatment followed by a prebake process. The prebake process results in regaining the hydrophobic nature of PDMS. The glass surface also becomes less hydrophilic after the prebake process. Smaller contact angle hysteresis of the glass substrate results in easier droplet movement during formation. Therefore, it will help to obtain a wider Dripping regime and higher monodispersity.

	Static angle ( $\theta_S$ )	Advancing angle ( $\theta_A$ )	Receding angle ( $\theta_R$ )
Glass	$60 \pm 4$	$69 \pm 5$	$52 \pm 5$
PDMS	$102 \pm 4$	$116 \pm 4$	$75 \pm 5$

desired hydrophobicity as well as solvent compatibility [40]. However, the chemicals used for this purpose are typically hazardous to work with. Moreover, applying a reproducible and uniform coating especially in confined microchannels is a challenge from the preparation perspective. Having a gaseous phase as the carrier fluid entirely eliminates the compatibility issue of PDMS in our system. Figure 2(A) represents the behavior of droplet formation after plasma treatment in this liquid-gas system. Droplets in this case show an affinity to ride on the side walls due to their hydrophilic condition after exposure to plasma. As a result, droplets are not capable of keeping their morphology during formation and tend to spread and form a liquid film on the side walls. To overcome this issue, we incorporated a high-temperature post-baking step instead of chemical treatment to achieve the surface conditions suitable for droplet generation in our system. Table 1 shows the measured contact angles for PDMS and glass substrates after the post-bake process. This technique ensures that all the PDMS walls regain their hydrophobic nature in a fast and uniform manner, minimizing the tendency of the droplets to adhere to the side walls (figure 2(B)).

In confined microfluidic channels droplet morphology is bounded by the microchannel dimensions. Thus, if the diameter of the generated droplet exceeds the height of the microchannel the droplet will be in contact with the top and bottom walls which result in additional interactions that influence the formation process. This condition occurred throughout the Dripping regime of our system. It has been observed that using a non-hydrophobic glass substrate as the bottom wall enables a more robust and reproducible dripping over a wider area of the flow map with higher monodispersity. We believe this behavior can

be related to the smaller contact angle hysteresis of a glass slide in comparison to a PDMS surface. For a Glass-PDMS combination, the net surface tension force is less than half of a fully PDMS microchannel. Therefore, droplets detach and move easier, especially at lower gas flow rates.

### Experimental setup

A custom microfluidic test setup has been developed for the experimental investigation of the gas-liquid droplet generation. The gas used as the continuous phase is supplied from a compressed air line. The air is passed through a desiccator and oil filter and is regulated in multiple steps before being routed into the microfluidic chip inlets. A master pressure regulator (up to 50 psi) reduces the pressure of the air followed by a low-pressure control valve (QPV1 Proportion-Air, up to 18 psi). For real-time monitoring of the air flow rate, an in-line mass flow meter (Sierra Smart-Trak2) is placed in the setup. A customized LabVIEW interface has also been developed for real-time control and data acquisition of the gaseous flow. Liquid flow control is provided by a glass syringe using a high precision syringe pump (PHD2000 Harvard Apparatus). Imaging and visualization of the formation process is facilitated using a high-speed CMOS camera (Photron SA5) which is mounted on an inverted microscope (Nikon Ti-U). Generated drops within the Dripping and Multi-Satellite Formation regimes are collected off the chip in a mixture of Hexadecane with 2.5 wt% of span 80, a nonionic surfactant (Sigma-Aldrich Corp.). The outlet of the microfluidic chip is cut and submerged in the oil bath. As a result, the generated droplets are collected downstream of the device outlet once they transition into the oil bath.

## Results and discussion

### Flow patterns

Unlike liquid-liquid droplet microfluidic systems that are usually characterized by the Capillary number ( $Ca$ ) of the two fluids [9, 12],  $Ca$  in our experiments always remained below 0.02. In contrast, the Reynolds number ( $Re$ ) for the continuous gaseous phase was in the range between 10 and 600 indicating the relevance of inertia in this system. However, such high  $Re$  and low  $Ca$  for all the flow conditions of the system do not clearly illuminate the fundamental mechanisms behind the different flow regimes. Therefore, we employed the Weber number ( $We$ ) to parametrize the droplet breakup processes as it changed in a moderate range in our experiments ( $We \equiv Re \cdot Ca$ ). Utilizing  $We$  led to a better characterization of the flow regimes presented in this system. The  $We$  number for both phases is defined as:

$$We = \frac{\rho U^2 D_H}{\sigma}$$

where  $\rho$  and  $\sigma$  are the fluid density and interfacial tension respectively. Air is used as the gaseous phase whose density throughout the experiments were calculated considering its compressible

flow effects inside the microchannels. Distilled water serves as the liquid phase.  $U$  is the average fluid velocity inside the channel at the junction which is calculated by dividing the flow rate by the cross section area, and  $D_H$  represents the hydraulic diameter of the rectangular cross section of the microchannel. The  $We$  for the gaseous phase ( $We_G$ ) is defined based on the throat cross section at the flow-focusing junction, and for the liquid phase  $We_L$  is defined based on the liquid channel dimensions. Using the aforementioned definitions,  $We_L$  is in the range 0.0001–0.3 and  $We_G$  in the range 0.008–25. These wide ranges of flow conditions result in various breakup modes which are explained in the following section.

Experiments on each chip were performed by initiating a gaseous flow inside the device to prevent the liquid from flooding the microchannels. Liquid water is subsequently injected into the flow-focusing junction. Mapping experiments were conducted by setting a specified liquid flow rate and increasing the gas flow rate. As such, the maps consist of multiple horizontal lines of a fixed liquid flow rate ( $We_L$ ), with transitions occurring as the gas flow rate ( $We_G$ ) is changed (increased). We conducted several experiments using multiple chips to account for wettability changes associated with the chips being exposed to large amount of water for a long period of time. Over a wide range of flow conditions we observed six distinct regimes which are defined as: Co-Flowing (■), Threading (◆), Plugging (▲), Dripping (●), Jetting (▶), and Multi-Satellite Formation (▼). A typical flow regime map depicting these different breakup modes is shown in figure 3 based on  $We_G$  and  $We_L$ . In this map the regions associated with each flow regime are distinguished with a different color. The gray areas in the plot represent the transition regions between two adjacent regimes. We used these finite transition regions rather than infinitesimally thin solid lines to depict the change in the flow regime more realistically. This is more consistent with the observations from experiments since flow regime transition could occur anywhere within the shaded regions from a statistical point of view, which is determined by the microfluidic chips and flow rate measurements in the experiments. However, dashed lines are also included in the flow map as a reference and guideline to distinguish between the actual flow regimes and intermediate transition regions. Furthermore, these lines can be considered as approximate boundaries between each two flow regime regions.

At low values of  $We_G$ , the flow is characterized by the formation of liquid threads that extend along the microchannel outlet. We observed that at low values of liquid flow (for  $We_L < 10^{-2}$ ), the formed thread does not remain stable along the outlet. In this region which is referred to as the Threading regime, an unstable thread extends downstream of the junction where it breaks up intermittently at different locations and results in multiple plugs and droplets. In the Co-flowing regime, which occurs at higher values of  $We_L$ , the liquid thread is stable and extends throughout the microchannel outlet. As the value of  $We_L$  increases, the thickness of this continuous liquid thread increases until it obstructs the microchannel outlet. A periodic breakup takes place at higher  $We_G$  where each formed thread is broken up into a single plug whose length

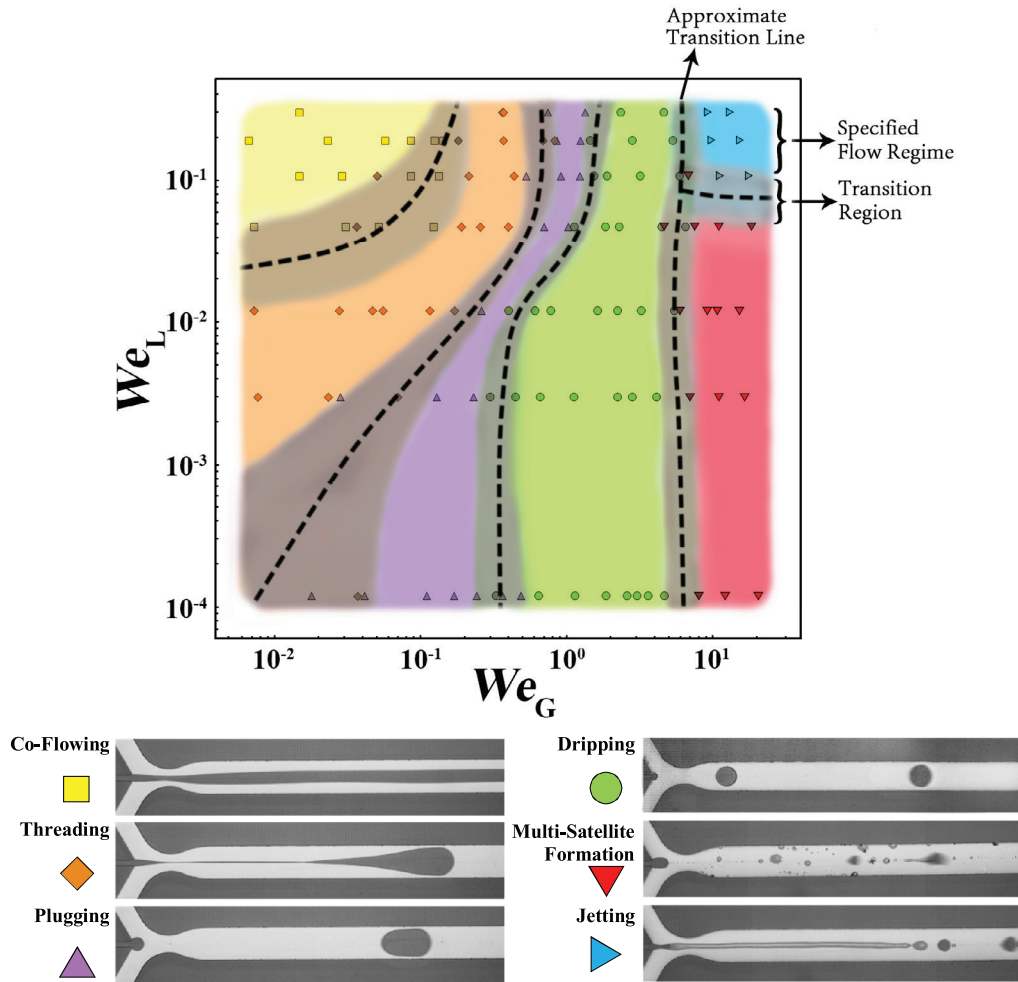


**Figure 3.** Flow regime map of water-in-air droplet formation in a planar flow-focusing microfluidic device. Different flow regions are distinguished with different colors. The transition between the flow regimes is also represented as a finite shaded region rather than a solid line to account for the uncertainties associated with the experiments and calculations of the  $We$  values.

is bigger than its width ( $L_{\text{plug}} > 2W_{\text{plug}}$ ). This corresponds to the Plugging region, with threads that break up very close to the flow-focusing junction at a distance  $L_{\text{breakup}} < 10W_{\text{outlet}}$  measured from the junction. The Dripping regime is observed beyond the Plugging regime when the inertia forces start balancing the surface tension forces at the junction (around  $We_G \approx 0.3$ ). In this regime, circular drops are formed at the junction which are highly-reproducible and uniform over a wide range of frequencies and sizes. Increasing  $We_G$ , however, creates a chaotic condition that involves unsteady and random droplet breakup dynamics. It can be seen from the flow map that a transition from the Dripping to the Multi-Satellite Formation regime occurs around  $We_G \approx 6$ . Beyond this point a polydisperse spray of the liquid is generated inside the microchannel. The Multi-Satellite Formation regime has not been previously reported in liquid-liquid systems since its appearance is mostly due to the highly inertial nature of the continuous phase which is usually negligible in oil-water systems. We observed that at higher liquid flows a long liquid jet is formed after the junction which breaks into individual droplets due to Rayleigh capillary instability [41]. In this Jetting regime, characterized by droplet tip streaming of an extended liquid jet, droplet generation is less controlled. However,

generated droplets are in the order of the liquid jet diameter and much smaller than the droplets from the Dripping regime.

In addition to the flow conditions, the geometry of the microchannel flow-focusing section plays an important role in the flow map characteristics of this system. We were interested on the influence that liquid microchannel size has on the Dripping regime in particular. Three different chips with liquid channel widths of  $25 \mu\text{m}$ ,  $50 \mu\text{m}$ , and  $100 \mu\text{m}$  were considered for this part. Flow mapping experiments were conducted for the wider liquid channels ( $50 \mu\text{m}$  and  $100 \mu\text{m}$ ) and the results are compared against the original flow map with the narrower liquid channel ( $25 \mu\text{m}$ ) as shown in figure 4. For these maps we have only included the approximate dashed lines to better compare the flow regimes layout together. It can be seen that increasing the liquid channel size results in a smaller Dripping region, which is highlighted with the green color in the flow map. Increasing the size of the liquid channel results in larger surface tension forces that hold the droplet during formation. Therefore, higher detaching forces are required to pinch-off the thread at the junction to create discrete droplets. This will shift the transition from the Threading and Plugging regimes to the Dripping regime to higher values of  $We_G$ . Transition to the Satellite Formation regime is less dependent on the liquid

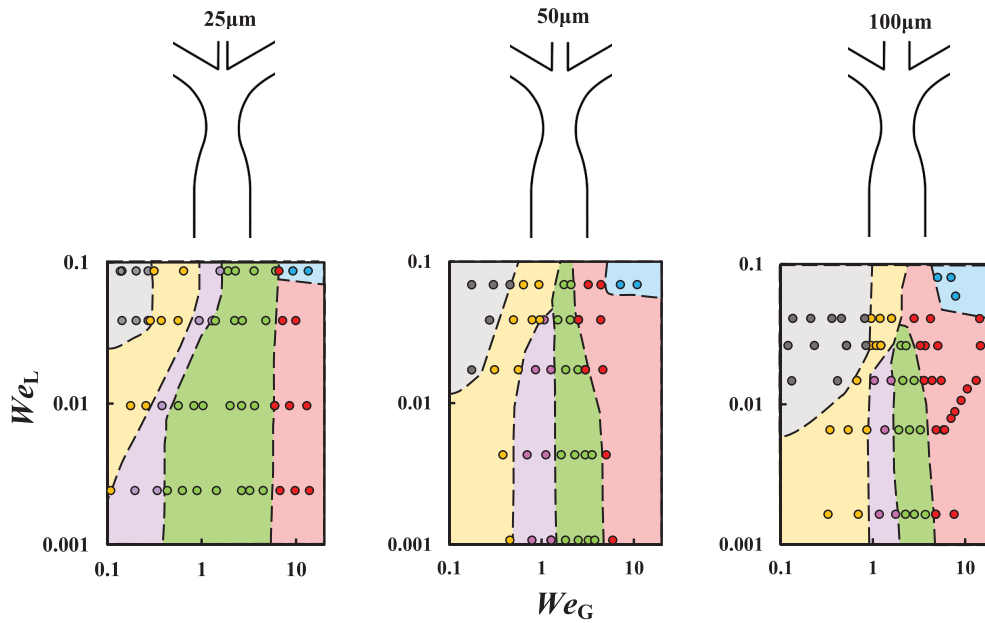


**Figure 4.** Comparison of the flow map for chips with different liquid channel sizes. The area for the Dripping region (the green region) is reduced as the liquid channel size increases. However, the Threading and Co-flow regions have expanded as a result of increase in the surface tensions force that holds the thread and prevents the detachment at lower gas flow rates.

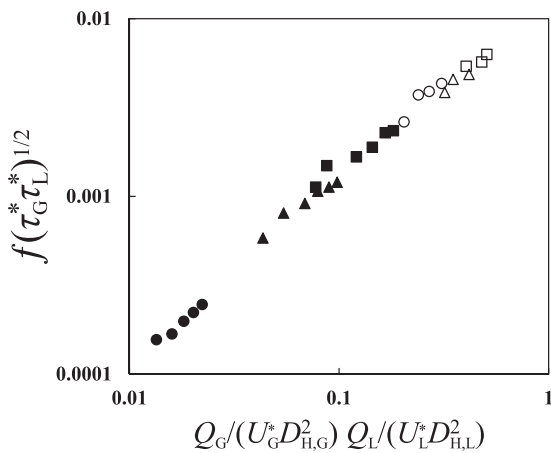


**Figure 5.** Experimental data of droplet generation frequency as a function of the product of liquid and gas flow rates. Frequency can be scaled as  $f \propto Q_G Q_L$ .

channel size since it is mostly due to the inertial effects of the gaseous phase. According to the flow maps, the Multi-Satellite Formation transition typically occurs around  $We_G \approx 6-7$  for all the chips. Consequently, increasing the size of the liquid channel would shrink the Dripping region by expanding the Threading and Co-flow region.

*Generation rate, droplet morphology, and monodispersity*

Three important aspects of the Dripping regime are investigated by characterizing the generation frequency, morphology of the droplets inside the microchannel, and monodispersity of the generated droplets within this region. The frequency of droplet formation ( $f_{\text{Generation}}$ ) is obtained by manually counting the number of droplets generated over a given time interval from the high-speed videos, and varies between less than 30 up to

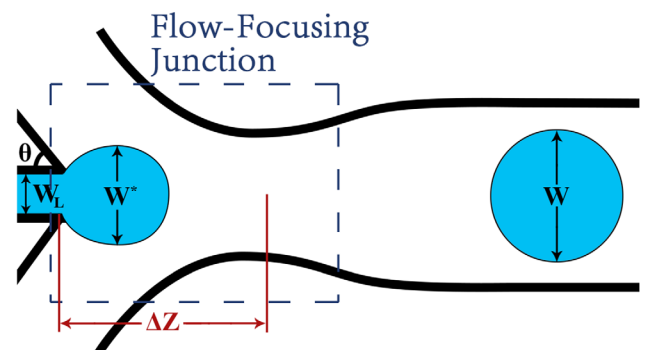


**Figure 6.** Schematic of the flow-focusing geometry and dimensions used in the droplet detachment analysis.

1000 Hz (drops per second) over the entire Dripping regime. Experimental measurements show that the frequency increases proportionally with both flow rates. Therefore, the frequency in this system can be scaled as the product of the two flow rates (i.e.  $f \propto Q_G Q_L$ ). Flow rates are non-dimensionalized by the characteristic inertial velocities ( $U^* = (\sigma/\rho D_H)^{1/2}$ ) obtained from a Weber number of unity for both phases. Similarly, a characteristic timescale ( $\tau^* = D_H/U^*$ ) can be used to non-dimensionalize the frequency. The results of this scaling are shown in figure 5.

During the course of the generation process, a droplet starts forming from the liquid microchannel in the flow-focusing junction. As the liquid is injected into the droplet volume, the droplet grows in the plane at the junction. The droplet is attached to the liquid microchannel by a surface tension force that can be scaled as,

$$F_\sigma \sim \sigma D_{H,L} \tag{1}$$

where  $D_{H,L}$  is the hydraulic diameter of the liquid microchannel. As the droplet protrudes into the junction, it experiences inertial forces of the high speed gaseous medium

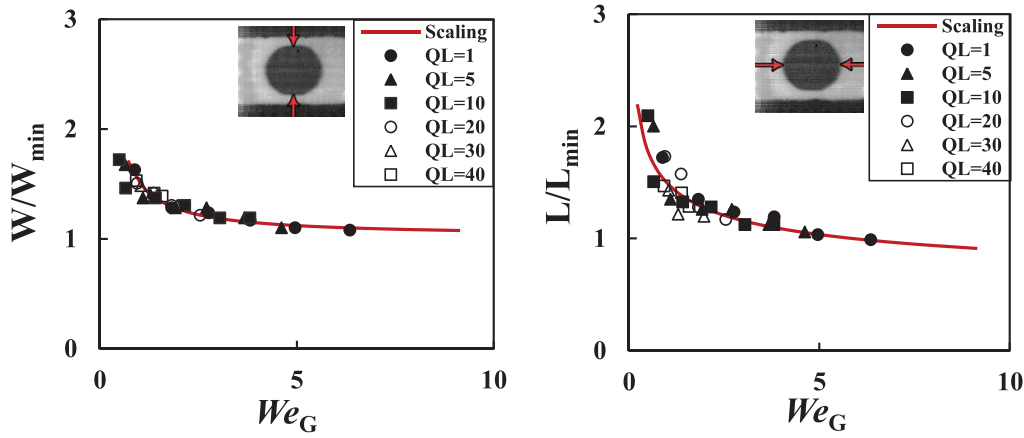


**Figure 7.** Droplet morphology normalized with the minimum width and length of the droplets in the Dripping regime as a function of gas Weber number ( $We_G$ ). Minimum droplet width and length are assumed to be equal values that are obtained based on the minimum volume of the prefilled droplet during the formation process at high gas flow rates where droplet tends to have a more circular morphology. This minimum is dependent on the geometry of the flow-focusing microchannel and is calculated to be about  $86 \mu\text{m}$  for the geometry used in our experiments.

that co-flows with the liquid droplet. The inertial force of the gaseous phase can be scaled as;

$$F_I \sim \frac{\rho Q_G^2}{D_{H,G}^4} h(W^* - W_L) \cos \theta \quad (2)$$

where  $D_{H,G}$  is the hydraulic diameter of the gas microchannel,  $h$  is the droplet height which is equal to the channel height,  $\theta$  is the angle at which the air enters the junction,  $W_L$  is the liquid microchannel width, and  $W^*$  is the droplet width during the formation stage (see figure 6). When the aforementioned forces balance, the droplet width can be approximated as  $W^* \sim \sigma D_{H,G}^4 / \rho Q_G^2 h \cos \theta + W_L$ . However, the morphology of the droplets was assessed from the images of the droplets moving inside the microchannel outlet after the droplets are detached. As such, a similar scaling dependence can be used for the measured width with respect to the inertial force but with a different proportionality factor and minimum width. To calculate this minimum width ( $W$ ), we consider the limiting case of  $W^* \approx W_L$  which occurs experimentally at high gas flow rates and also from the scaling equation. In this case, the prefilled droplet volume in the junction forms a rectangular liquid ligament whose width is in the order of the liquid microchannel width and the length is stretched to the throat of the junction ( $\Delta Z$ ). This volume results in minimum droplet width of  $86 \mu\text{m}$  after detachment, assuming a circular morphology for these droplets at high gas flow rates, which is a reasonable assumption based on the experimental data. Since the complete generation process always starts with the prefilling process, this obtained droplet size can be considered the minimum width and length that can be achieved within the Dripping regime. Therefore, droplet width can be calculated as  $W = C_1 \sigma / \rho Q_G^2 + C_2$ , where  $C_1$  takes into account the geometrical parameters and a fitting factor, and  $C_2$  is the minimum droplet width that can be achieved in the Dripping regime of this system.

The volume of the droplet in the dripping regime can be related to the generation frequency and the liquid flow rate via conservation of mass of the liquid flow,

$$V_{\text{droplet}} = \frac{Q_L}{f} \quad (3)$$

If the droplet is assumed to have a relatively uniform width over its entire length, the volume of the droplet is proportional to the product of its dimensions. Therefore, the volume can be approximated as  $V_{\text{droplet}} \propto LWh$ , where  $L$ ,  $W$ , and  $h$  are the droplet length, width, and height, respectively. In order to be consistent with the assumed (and mostly observed) droplet volume, experimental data for the measured length were corrected in some cases where the droplet contained a morphology with non-uniform width. By substituting the aforementioned scaling for the frequency ( $f \propto Q_G Q_L$ ), droplet length can be scaled as  $L \sim 1/hWQ_G$ . Figure 7 shows the normalized droplet morphology using the minimum values obtained in the Dripping regime as a function of the  $We_G$ . It can be seen that both droplet length and width decrease with increasing gas flow. However, the effect of liquid flow rate is less discernable in the morphology and more pronounced in the formation frequency.

Generated droplets are collected off the chip in a glass vial filled with a different liquid which is immiscible with the water droplets. Captured images from the collected droplets were processed using a customized MATLAB program to analyze the size of the drops and their distribution. Since the droplets are spherical after transitioning into the liquid medium, we use the droplets' diameter as the characteristic length scale in this part. Comparison between droplets in the Dripping and Multi-Satellite Formation regions is shown in figure 8. Size uniformity of the collected droplets within the Dripping regime demonstrates the controlled generation of the droplets within this region. The generated droplets have a polydispersity index (PDI) defined as  $\sigma/d$  (where  $\sigma$  represents the standard deviation of the droplet diameters and  $d$  is the average diameter of the generated drops), of less than 5%. Droplets generated in the Dripping regime can form a uniform closely-packed structure inside the liquid medium as shown in the figure. Multi-Satellite Formation regime, however, results



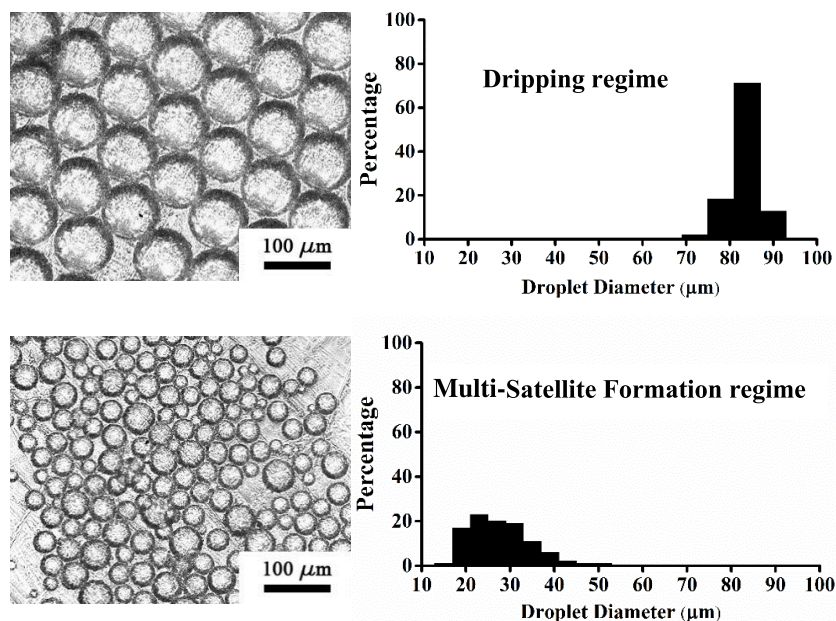


**Figure 8.** Actual images and size distributions of samples of 500 collected droplets within the Dripping and Multi-Satellite Formation regimes. Liquid flow rate for both cases is  $5 \mu\text{l min}^{-1}$ . Multi-Satellite Formation regime is obtained at higher  $We_G$  according to the flow map. In the Dripping region the generated droplets are uniform in size. In the Multi-Satellite Formation regime, however, small daughter droplets are generated beside the main droplet which results in polydisperse distribution of the droplets.

in polydisperse droplets which are distributed over a wide range of diameters even for a fixed flow condition.

## Conclusions

Controlled generation of liquid droplets in microfluidic networks is an area of huge promise for a variety of applications in biochemistry and material science. Droplet-based microfluidic devices typically employ dispersions of one liquid within a continuous immiscible liquid phase, such as the creation of uniform water-in-oil emulsions. Generation of aqueous liquid droplets using a continuous gaseous phase has been recently demonstrated within microfluidic devices. This approach provides great potentials in modern lab-on-a-chip systems for high-throughput production of oil-free particles and airborne microreactors. In this work we investigated different aspects of controlled formation of uniform micrometer-sized water droplets in air using a microfluidic flow-focusing device. The droplet generation module is fabricated following standard soft lithography techniques with PDMS. A standard microscope glass slide acts as the bottom surface on which each device is bonded using a lab-scale plasma cleaner. Microfluidic devices are finally post-baked at high temperatures for several hours. The hydrophilic bottom wall (glass) creates a mixed surface condition inside the microchannel since the post bake step renders the PDMS walls highly hydrophobic. By using a PDMS-glass hybrid structure, we found six different flow regimes in this system: Co-flowing, Threading, Plugging, Dripping, Jetting, and Multi-Satellite Formation. We further investigated the Dripping regime which corresponds to controlled generation of monodisperse droplets at the flow-focusing junction inside the microchannel. It was shown

that increasing the liquid channel size results in a smaller Dripping regime. Generation rate, droplet morphology, and monodispersity of the droplets were investigated for different liquid and air flows within the Dripping regime. Results of this work demonstrate smaller droplets (less than  $100 \mu\text{m}$ ) at higher generation rates (up to  $1 \text{ kHz}$ ) that are highly uniform in size ( $PDI < 5\%$ ) which shows a significant improvement for liquid-in-gas microfluidic systems. The contributions presented in this article provide practical guidelines towards creating oil-free uniform droplets that can be used as templates for microparticle and microfiber synthesis with control on the size and frequency. Moreover, many biochemically relevant applications can also benefit from uniform digitization of sample within a gaseous medium, namely for aerosol drug delivery and high-throughput screening of targets from gaseous media.

## Acknowledgments

This work has been funded with an NSF CAREER Award grant CBET-1522841.

## References

- [1] Lagus T P and Edd J F 2013 A review of the theory, methods and recent applications of high-throughput single-cell droplet microfluidics *J. Phys. D: Appl. Phys.* **46** 114005
- [2] Casadevall i Solvas X and deMello A 2011 Droplet microfluidics: recent developments and future applications *Chem. Commun.* **47** 1936–42
- [3] Nunes J K, Tsai S S H, Wan J and Stone H A 2013 Dripping and jetting in microfluidic multiphase flows applied to particle and fiber synthesis *J. Phys. D: Appl. Phys.* **46** 114002

- [4] Thorsen T, Roberts R W, Arnold F H and Quake S R 2001 Dynamic pattern formation in a vesicle-generating microfluidic device *Phys. Rev. Lett.* **86** 4163–6
- [5] Anna S L, Bontoux N and Stone H A 2003 Formation of dispersions using ‘flow focusing’ in microchannels *Appl. Phys. Lett.* **82** 364–6
- [6] Christopher G F and Anna S L 2007 Microfluidic methods for generating continuous droplet streams *J. Phys. D: Appl. Phys.* **40** R319–36
- [7] Nie Z, Seo M, Xu S, Lewis P C, Mok M, Kumacheva E, Whitesides G M, Garstecki P and Stone H A 2008 Emulsification in a microfluidic flow-focusing device: effect of the viscosities of the liquids *Microfluid. Nanofluid.* **5** 585–94
- [8] Lee W, Walker L M and Anna S L 2009 Role of geometry and fluid properties in droplet and thread formation processes in planar flow focusing *Phys. Fluids* **21** 032103
- [9] Carneiro J, Doutel E, Campos J B L M and Miranda J M 2016 PDMS droplet formation and characterization by hydrodynamic flow focusing technique in a PDMS square microchannel *J. Micromech. Microeng.* **26** 1–8
- [10] Zhu P and Wang L 2016 Passive and active droplet generation with microfluidics: a review *Lab Chip* **17** 34–75
- [11] Baroud C N, Gallaire F and Dangla R 2010 Dynamics of microfluidic droplets *Lab Chip* **10** 2032–45
- [12] Cubaud T and Mason T G 2008 Capillary threads and viscous droplets in square microchannels *Phys. Fluids* **20** 53302
- [13] Martín-Banderas L, Flores-Masquera M, Riesco-Chueca P, Rodríguez-Gil A, Cebolla Á, Chávez S and Gañán-Calvo A M 2005 Flow focusing: a versatile technology to produce size-controlled and specific-morphology microparticles *Small* **1** 688–92
- [14] Roach L S, Song H and Ismagilov R F 2005 Controlling nonspecific protein adsorption in a plug-based microfluidic system by controlling interfacial chemistry using fluorosurfactants *Anal. Chem.* **77** 785–96
- [15] Skhiri Y *et al* 2012 Dynamics of molecular transport by surfactants in emulsions *Soft Matter* **8** 10618
- [16] Acero a J, Rebollo-Muñoz N, Montanero J M, Gañán-Calvo a M and Vega E J 2013 A new flow focusing technique to produce very thin jets *J. Micromech. Microeng.* **23** 65009
- [17] Acero a J, Montanero J M, Ferrera C, Herrada M A and Gañán-Calvo A M 2012 Enhancement of the stability of the flow focusing technique for low-viscosity liquids *J. Micromech. Microeng.* **22** 115039
- [18] Luque A, Perdignes F, Estevé J, Montserrat J, Gañán-Calvo A and Quero J M 2009 Reduction of droplet-size dispersion in parallel flow-focusing microdevices using a passive method *J. Micromech. Microeng.* **19** 45029
- [19] Gañán-Calvo A 1998 Generation of steady liquid microthreads and micron-sized monodisperse sprays in gas streams *Phys. Rev. Lett.* **80** 285–8
- [20] Gordillo J M, Pérez-Saborid M and Gañán-Calvo A M 2001 Linear stability of co-flowing liquid–gas jets *J. Fluid Mech.* **448** 23–51
- [21] Acero A J, Ferrera C, Montanero J M and Gañán-Calvo A M 2012 Focusing liquid microjets with nozzles *J. Micromech. Microeng.* **22** 65011
- [22] Anna S L 2016 Droplets and bubbles in microfluidic devices *Annu. Rev. Fluid Mech.* **48** 285–309
- [23] Fang C, Hidrovo C, Wang F, Eaton J and Goodson K 2008 3-D numerical simulation of contact angle hysteresis for microscale two phase flow *Int. J. Multiph. Flow* **34** 690–705
- [24] Cheah M J, Kevrekidis I G and Benziger J B 2013 Water slug to drop and film transitions in gas-flow channels *Langmuir* **29** 15122–36
- [25] Cheah M J, Kevrekidis I G and Benziger J B 2013 Water slug formation and motion in gas flow channels: the effects of geometry, surface wettability, and gravity *Langmuir* **29** 9918–34
- [26] Kim D R, Koo J M, Fang C, Steinbrenner J E, Lee E S, Wang F M, Hidrovo C H, Eaton J K and Goodson K E 2007 Compact model of slug flow in microchannels *ASME 5th Int. Conf. on Nanochannels, Microchannels, and Minichannels* pp 321–9
- [27] Schillberg C H and Kandlikar S G 2007 A review of models for droplet detachment from the gas diffusion layer-gas flow channel interface in PEMFCs *ASME 5th Int. Conf. on Nanochannels, Microchannels, and Minichannels* pp 299–310
- [28] Mukherjee A and Kandlikar S G 2006 A numerical analysis of growing water droplet inside an air supply channel of a PEM fuel cell *ASME Int. Mechanical Engineering Congress and Exposition, Fluids Engineering* pp 131–6
- [29] Lee E S, Hidrovo C H, Steinbrenner J E, Wang F-M, Vigneron S, Goodson K E and Eaton J K 2005 Flow structures and frictional characteristics on two-phase flow in microchannels in PEM fuel cells *ASME Fluids Engineering Division Summer Meeting* vol 1 pp 899–906
- [30] Koz M and Kandlikar S G 2013 Numerical investigation of interfacial transport resistance due to water droplets in proton exchange membrane fuel cell air channels *J. Power Sources* **243** 946–57
- [31] Steinbrenner J E, Lee E S, Hidrovo C H, Eaton J K and Goodson K E 2011 Impact of channel geometry on two-phase flow in fuel cell microchannels *J. Power Sources* **196** 5012–20
- [32] Zhu X, Sui P C and Djilali N 2008 Numerical simulation of emergence of a water droplet from a pore into a microchannel gas stream *Microfluid. Nanofluid.* **4** 543–55
- [33] Hidrovo C H, Wang F-M, Steinbrenner J E, Lee E S, Vigneron S, Cheng C-H, Eaton J K and Goodson K E 2005 Water slug detachment in two-phase hydrophobic microchannel flows *ASME 3rd Int. Conf. on Microchannels and Minichannels* pp 709–15
- [34] Carroll B and Hidrovo C 2013 Droplet detachment mechanism in a high-speed gaseous microflow *J. Fluids Eng.* **135** 71206
- [35] Jiang K, Lu A X, Dimitrakopoulos P, DeVoe D L and Raghavan S R 2015 Microfluidic generation of uniform water droplets using gas as the continuous phase *J. Colloid Interface Sci.* **448** 275–9
- [36] Shahriari A, Kim M M, Zamani S, Phillip N, Nasouri B and Hidrovo C H 2016 Flow regime mapping of high inertial gas–liquid droplet microflows in flow-focusing geometries *Microfluid. Nanofluid.* **20** 20
- [37] Xia Y and Whitesides G M 1998 Soft lithography *Annu. Rev. Mater. Sci.* **28** 153–84
- [38] Rotem A, Abate A R, Utada A S, Van Steijn V and Weitz D A 2012 Drop formation in non-planar microfluidic devices *Lab Chip* **12** 4263
- [39] Lee J N, Park C and Whitesides G M 2003 Solvent compatibility of poly(dimethylsiloxane)-based microfluidic devices *Anal. Chem.* **75** 6544–54
- [40] Wong I and Ho C-M 2009 Surface molecular property modifications for poly(dimethylsiloxane) (PDMS) based microfluidic devices *Microfluid. Nanofluid.* **7** 291–306
- [41] Anna S L and Mayer H C 2006 Microscale tipstreaming in a microfluidic flow focusing device *Phys. Fluids* **18** 121512